

Synthesis of efficient iron phosphide catalyst for electrocatalytic hydrogen generation

T. Chouki¹, D. Lazarević², B. V. Donkova³, S. Emin^{1*}

¹Materials Research Laboratory, University of Nova Gorica, Vipavska 11c, 5270, Ajdovščina, Slovenia

²Faculty of Sciences, Department of Chemistry, University of Novi Sad, 21000, Novi Sad, Serbia

³Faculty of Chemistry and Pharmacy, University of Sofia, 1 James Bourchier Blvd., 1164, Sofia, Bulgaria

Received: September 25, 2020; Revised: September 29, 2020

A solvothermal synthesis of iron phosphide electrocatalysts using triphenylphosphine (TPP) as phosphorus precursor is presented. The synthetic protocol generates Fe₂P/FeP phase at 350°C. After deposition of the catalyst onto graphite substrate heat-treatment at higher temperature was carried out. Annealing at 500°C under reductive atmosphere induced structural changes in the Fe₂P/FeP samples which yielded a pure Fe₂P phase. The electrocatalytic activity of the Fe₂P catalyst was studied for hydrogen evolution reaction (HER) in 0.5 M H₂SO₄. The recorded overpotential for HER was about 130 mV vs. a reversible hydrogen electrode (RHE) at 10 mA cm⁻².

Keywords: solvothermal synthesis; iron phosphide; electrocatalyst; hydrogen evolution; overpotential

INTRODUCTION

It has been demonstrated that transition metal phosphides (TMPs) such as iron phosphides [1, 2], cobalt phosphides [3], nickel phosphides [4], molybdenum phosphides [5], and tungsten phosphides [6], among others, are efficient electrocatalysts for hydrogen evolution reaction (HER). TMPs are considered as alternative catalysts to platinum group metals because of their abundance, low cost, and high catalytic activity [7]. Usually, traditional methods, such as chemical vapor deposition (CVD), temperature-programmed reduction (TRP), or solvothermal synthesis, are used to synthesize TMPs [8, 9]. In CVD, volatile precursors decompose on a heated substrate and give the corresponding class of materials like TMPs. The TRP approach is based on the reduction of metal phosphates using hydrogen gas. However, both CVD and TRP have limitations because these require expensive equipment [10] and high temperatures (~600 – 900°C) during the reaction process. The solvothermal technique is a preferred way for preparation of TMPs at low temperatures based on the reaction of a metal precursor with phosphorus (P)-containing reagents [9] such as trioctylphosphine (TOP), red phosphorus [11], tributyl phosphine (TBP) [12], tri-*n*-octylphosphine oxide (TOPO) [13], and tris(diethylamino) phosphine (TEAP) [12]. Among these P-precursors, TOP was the most studied for the synthesis of iron phosphides (Fe₂P and FeP) [14, 15], cobalt phosphide (CoP) [3], nickel phosphide (Ni₂P) [16], molybdenum phosphide (MoP) [17], tungsten phosphide (WP) [6], etc.

However, TOP and most of the cited above precursors are expensive, toxic, and unstable in air. To overcome these limitations, triphenylphosphine (TPP) and triphenyl phosphite (TPOP) were introduced in the synthesis of TMPs [18]. TPP possesses moderate stability against oxidation in air and has been used for synthesis of TMPs in Ullmann-type reactions with ferrocene in vacuum-sealed tubes [19] or open-tube furnaces in an inert atmosphere at 350 to 400°C [20]. The application of TPP in solvothermal synthesis of TMPs was demonstrated for cobalt phosphide (Co₂P) NPs [21], nickel phosphide (Ni_xP_y) NPs [22] and for Fe₂P and FeP NPs in our previous study [23]. However, little is known about the preparation of mixed Fe₂P/FeP phases using TPP precursor and their use in HER studies.

Herein, we report the solvothermal synthesis of iron phosphide microspheres (MS) using a TPP precursor. At the conditions applied the synthesis procedure generated Fe₂P/FeP MS. With the goal to test the obtained Fe₂P/FeP MS in HER studies these were spin-coated onto graphite substrate and heat-treated under reductive (Ar:H₂) atmosphere. However, the heat treatment caused structural transformations of mixed Fe₂P/FeP to Fe₂P phase. The electrocatalytic tests showed that the obtained Fe₂P phase is an efficient catalyst for HER.

EXPERIMENTAL

Materials

Iron pentacarbonyl (>99.99%, Fe (CO)₅), OLA (70%), ethanol (98%, EtOH), acetone (95%), and sulfuric acid (97%, H₂SO₄) were purchased from Sigma-Aldrich. TPP (99%), SQ (98%), and chloroform (99.5%, CHCl₃) were purchased from

* To whom all correspondence should be sent:

E-mail: saim.emin@ung.si

© 2021 Bulgarian Academy of Sciences, Union of Chemists in Bulgaria

Alpha Aesar (United Kingdom). A graphite block (99.9%) used as a substrate was obtained from Beijing Great Wall Co., Ltd. (China).

Synthesis of Fe₂P/FeP MS and preparation of Fe₂P catalyst

The synthesis of Fe₂P/FeP NPs was achieved under the following conditions: 0.6 g of Fe(CO)₅, 3.14 g of TPP, 3 ml of OLA, and 8 ml of SQ were mixed in a 100 ml three-neck flask (Ar atmosphere) and heated at 150°C (ramp rate: 10°C/min) until the TPP was dissolved. Later, the reaction temperature was increased and kept at 350°C for 15 min. After cooling the suspension, the product was isolated by adding a mixture of solvents (10 ml, ethanol/acetone –v/v, 1:1). Following centrifugation at 8000 rpm for 5 min and decantation of the solution, the Fe₂P/FeP product was isolated as a solid material. After this the solid mass was dried at 50°C for 30 min, roughly 0.27 g of powder was obtained. The obtained iron phosphide powder (e.g., 0.27 g) was dispersed in 2 ml of CHCl₃ and spin-coated on graphite at 600 rpm for 20 s. To remove the organics from the surface heat treatment of the Fe₂P/FeP thin film was conducted at 500°C for 30 min (heating ramp: 10°C min⁻¹) in a muffle furnace under a mixture of Ar:H₂ gasses (65:35 % v/v, Inoxline H35, Messer) where the gas flow rate was adjusted to 3 L min⁻¹. In our earlier studies we found that it is essential to use a mixture of gases and the cited above ratio to produce active catalyst for HER [23]. The amount of catalyst loaded onto the graphite was in the range of 20 mg cm⁻².

Characterization

The morphology of the catalyst was studied using a scanning electron microscope (JEOL JSM 7100 F). Transmission electron microscopy (TEM) study of Fe₂P/FeP particles was carried out using a JEOL 2100F microscope at an accelerating voltage of 200 kV. X-ray diffraction (XRD) studies were performed using the MiniFlex 600 (Rigaku) and the diffractograms were analyzed using the PDXL software package, Ver. 1.4. Rietveld analysis of the mixed Fe₂P/FeP phase was carried out using the MAUD software [24]. All electrochemical measurements were performed using a potentiostat (EDAQ SP1) in a typical three-electrode system, in a 0.5 M H₂SO₄ aqueous solution (pH ≈ 0). Linear sweep voltammetry (LSV) tests were performed using Ag/AgCl (Sigma-Aldrich) as the reference electrode, iron phosphide-coated graphite substrates as the working electrodes, and graphite as the counter electrode with a scan rate of 5 mV s⁻¹. Experimentally measured potentials were converted

to a reversible hydrogen electrode (*E*_{RHE}) scale using the following equation:

$$E_{RHE} = E_{Ag/AgCl} + E^0_{Ag/AgCl} + (0.059 \times \text{pH}),$$

where *E*_{Ag/AgCl} is the measured potential vs. Ag/AgCl and *E*⁰_{Ag/AgCl} = 0.197 V is the standard potential of the Ag/AgCl reference electrode vs. RHE (at 25°C). Charge-transfer resistance was accessed using EIS measurements in 0.5 M H₂SO₄, at various applied potentials from –0.35 to –0.6 V vs. Ag/AgCl and frequencies from 100 to 1 MHz (10 mV AC dither).

RESULTS AND DISCUSSION

The XRD pattern (Fig. 1) of the not well crystallized mixed Fe₂P/FeP sample shows characteristic diffraction peaks at 41.05°, 44.33°, and 48°, which matched (111), (201) and (210) plane peaks of hexagonal Fe₂P (*P* $\bar{6}2m$, PDF# 1008826).

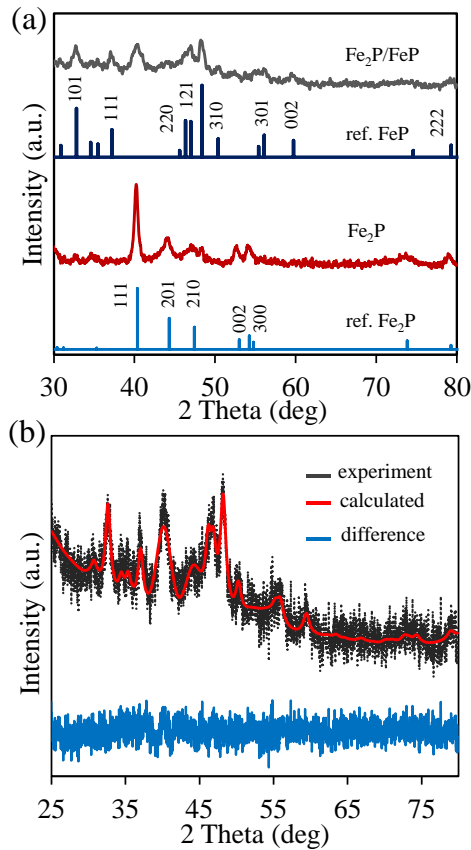


Fig. 1. (a) XRD patterns of Fe₂P/FeP synthesized at 350°C and Fe₂P obtained after the heat-treatment at 500°C. The XRD patterns of reference phases are given with labels. (b) Rietveld refinement of the mixed Fe₂P/FeP sample.

The calculated crystal lattice parameters *a* = *b* = 5.8220 ± 0.0070 Å and *c* = 3.5204 ± 0.0061 Å show a good agreement with existing literature values for hexagonal Fe₂P. The XRD diffraction peaks at 32.8°, 46.3°, and 48.38° are typical for the (101), (211), and

(121) planes of the orthorhombic FeP phase (*Pbnm*, PDF# 9008932). The determined crystal lattice parameters are equal to $a = 5.8097 \pm 0.0041 \text{ \AA}$, $b = 5.2042 \pm 0.0031 \text{ \AA}$, and $c = 3.1091 \pm 0.0018 \text{ \AA}$. The crystallite size calculated using the Williamson-Hall (W-H) method yielded an average size of $9.2 \pm 0.4 \text{ nm}$ for Fe₂P and $13.6 \pm 0.3 \text{ nm}$ for FeP samples. The calculated microstrain ($\times 10^{-5}$) was found as $1.63 \pm 0.03 \text{ a.u.}$ (FeP) and $2.2 \pm 0.02 \text{ a.u.}$ (Fe₂P). The mean crystallite size of Fe₂P and FeP estimated by W-H method and Scherrer's equation [25] is highly

intercorrelated in the frame of standard deviation. The Rietveld quantification gives a weight ratio of different phases in the as-synthesized Fe₂P/FeP sample equal to $45.1 \pm 2.4 \%$ (Fe₂P) and $54.9 \pm 2.4 \%$ (FeP). The heat-treatment process under reductive atmosphere converted the mixed Fe₂P/FeP to pure hexagonal Fe₂P (*P $\bar{6}$ 2m*, PDF# 1008826) where the calculated crystallite size of Fe₂P is 14.7 nm .

TEM images of iron Fe₂P/FeP particles are shown in Fig. 2.

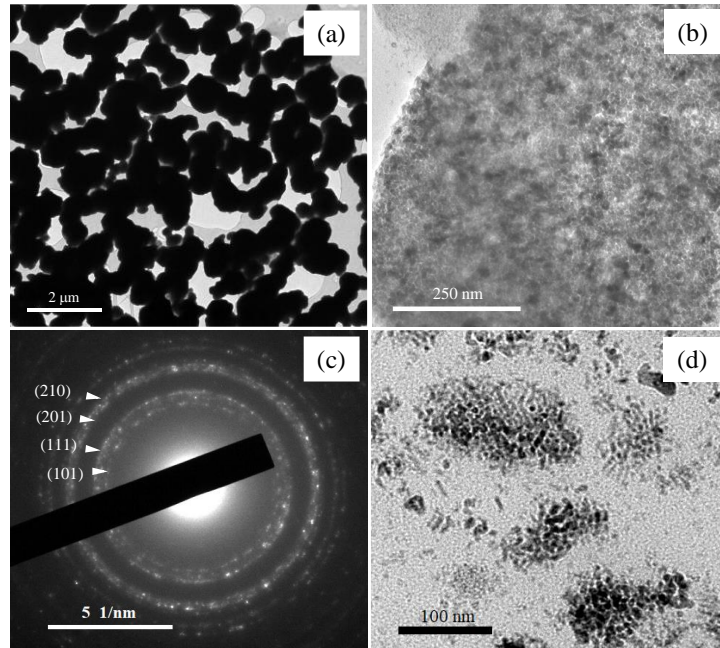


Fig. 2. (a,b,d) TEM images of Fe₂P/FeP particles at different magnifications. (c) The SAED is taken from the image in (b).

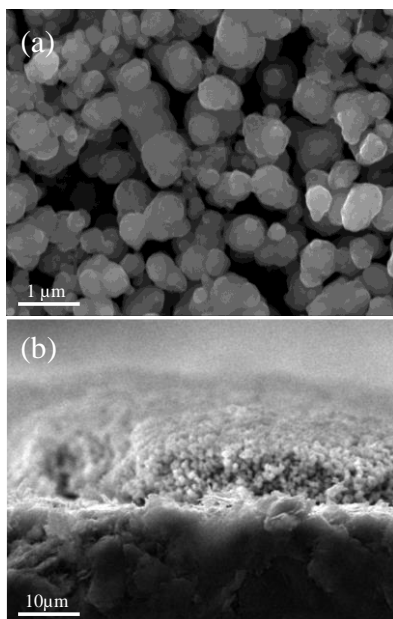


Fig. 3. SEM images of Fe₂P thin film in (a) top- and (b) cross-section views.

Detailed analysis of the obtained Fe₂P/FeP sample confirmed the presence of microspheres (MS) (Fig. 2a). The agglomerates in the TEM image do not reveal the real morphology since these are composed of individual Fe₂P/FeP MS. Closer look of the agglomerates show that these MS are made of small Fe₂P/FeP nanoparticles (NPs) with sizes in the range of 10 to 30 nm (Figs. 2b, d). The selected area electron diffraction (SAED) pattern confirms that the Fe₂P/FeP NPs are polycrystalline (Fig. 2). The lattice fringes in SAED image are equal to 2.835, 2.415 and 2.083 Å and correspond to (101), (111) and (201) planes for the Fe₂P and FeP. Figure 3 shows SEM images of Fe₂P MPs obtained after spin-coating of Fe₂P/FeP chloroform suspension onto graphite substrate and heat-treatment stage. The typical size range of Fe₂P microspheres is between 200 - 1000 nm (e.g. 1 μm). The average film thickness determined from the cross-section profile is close to $\sim 10 \text{ μm}$ (Fig. 3b).

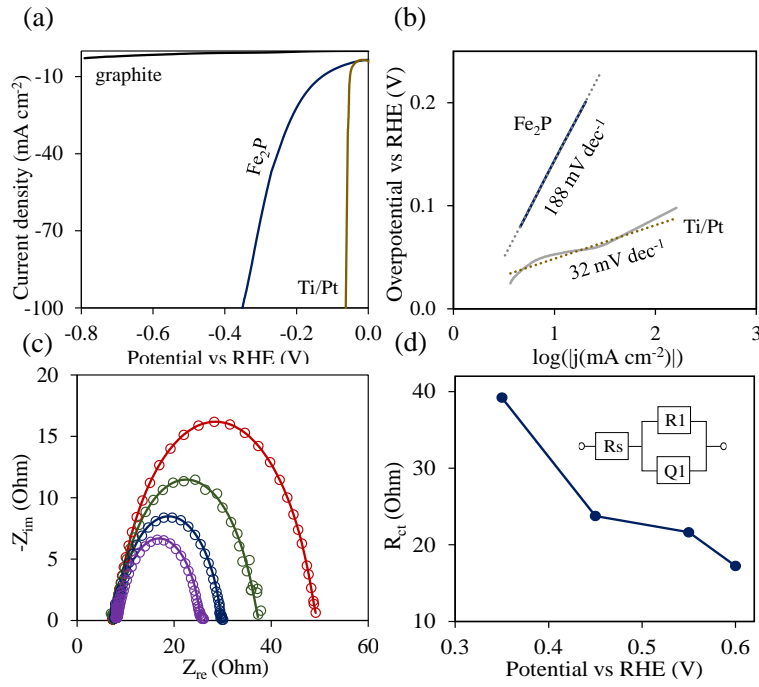


Fig. 4. (a) LSV characteristics (*iR*-corrected) of Fe₂P catalyst recorded at 5 mV s⁻¹ in 0.5 M H₂SO₄. For comparison, the pure graphite and a reference Ti/Pt electrode are also given. In (b) the Tafel plots of Fe₂P and Ti/Pt are given. In (c), EIS characteristics of Fe₂P. (d) Plot of *R*_{ct} vs. potential (negative values) for Fe₂P. The inset in (d) is a circuit element used to fit the EIS data.

Table 1. Selected summary of the HER performance of some iron phosphide particles in 0.5 M H₂SO₄. The overpotential of the electrocatalyst at a current density of 10 mA cm⁻² (*η*₁₀).

| Material | P source | Tafel slope (mV dec ⁻¹) | <i>η</i> ₁₀ (mA cm ⁻²) | Ref. |
|----------------------------|--|-------------------------------------|---|-------------------|
| FeP NPs/Ti | TOP | 37 | 50 | [15] |
| FeP NAs/CC | NaH ₂ PO ₂ | 45 | 58 | [26] |
| FeP@GPC | NaH ₂ PO ₂ | 68 | 72 | [27] |
| FeP NAs/Ti | NaH ₂ PO ₂ | 60 | 85 | [28] |
| FeP NWs array | (PH ₃) gas | 39 | 96 | [29] |
| FeP _x -300 | NaH ₂ PO ₂ | 64 | 100 | [30] |
| FeP NR | (NaH ₂ PO ₂ ·H ₂ O) | 54 | 107 | [31] |
| Fe ₂ P/FeP | TPP | 119 | 110 | [23] |
| HMFeP@C | PB | 56 | 115 | [32] |
| FeP NRs | NaH ₂ PO ₂ | 55 | 120 | [1] |
| Fe₂P NPs | TPP | 188 | 130 | This study |
| FeP NPs | TOP | 64 | 135 | [14] |
| FeP NPs | NaH ₂ PO ₂ | 65 | 154 | [33] |
| FeP NWs - free | (PH ₃) gas | 66 | 193 | [29] |
| Fe ₂ P@APC | NaH ₂ PO ₂ | 90 | 196 | [27] |
| FeP NSs | TOP | 67 | 235 | [34] |
| FeP _x -Ca | NaH ₂ PO ₂ | 105 | 263 | [30] |
| Bulk FeP | NaH ₂ PO ₂ | 82 | 285 | [1] |

Legend: PC – porous carbons; NAs – nanorod arrays; Ca – calcination; CC – nanorod arrays on carbon cloth; GPC – graphitic carbon; NWs – nanowires; NRs – nanorods; NS – nanosheets; APC – amorphous carbon; and NPC – nitrogen & phosphorus co-doped carbon.

The HER performance of the iron phosphide catalyst is presented in Fig. 4. LSV characteristics of Fe₂P recorded in 0.5 M H₂SO₄ revealed 130 mV at 10 mA cm⁻². The recorded overpotential of 130 mV for Fe₂P was found to be smaller than that of many iron phosphide electrocatalysts reported in the literature (Table 1). Another useful metric for interpreting polarization curves is the Tafel plot which indicates potential vs. log|j| (current in logarithm) [35]. In terms of the Volmer limiting step, the Tafel slope provides illustrative information for the comparison of the kinetic rate for the proton discharge reaction: H⁺ + e⁻ + M → H_{ad}-M. The Tafel slopes of Ti/Pt (reference) and Fe₂P were 32 and 188 mV dec⁻¹, respectively (Fig. 4b). As a rule, the lower the Tafel slope, the better is the catalytic performance of the material. The higher Tafel slope observed in this study can be attributed to the rate-limiting steps associated with H⁺ (adsorption)/H₂ (desorption) to different parameters such as exposed crystallographic facets, anionic/cationic vacancies, etc. [36]. EIS was used to determine the contribution of the Fe₂P catalyst toward HER at different applied potentials [21]. Figs. 4c, d show Nyquist plots for Fe₂P in 0.5 M H₂SO₄, recorded with a bias from -150 to -400 mV vs. RHE. The electrical circuit used to fit the data was assumed to be made of sheet resistance (R_s), contact phase (Q1) and resistance (R1) elements (Fig. 4d). At the surface of the electrode, the kinetics of electrochemical reaction was governed by charge-transfer resistance (R_{ct}) [21]. Fig. 4d shows the R_{ct} values obtained from the fitted semi-circles as a function of applied bias. At high overpotentials, the observed drop of R_{ct} was the result of the faster charge-transfer kinetics for HER [21]. EIS measurements of the Fe₂P film showed a low R_{ct} of 11 Ohms cm² which indicated efficient catalytic activity toward HER.

CONCLUSIONS

Fe₂P/FeP catalyst was successfully synthesized using a low-cost TPP precursor. The obtained iron phosphide particles were spin-coated on a graphite substrate and heat-treated at 500°C. Heating of the Fe₂P/FeP sample under reductive atmosphere yielded Fe₂P phase. The overpotential for HER recorded with Fe₂P catalyst in this study was comparable with or lower than most state-of-the-art iron phosphide catalysts. EIS measurements revealed that iron phosphide samples showed low charge-transfer resistance (R_{ct}) of 11 Ohms cm² which was ascribed to efficient HER.

Acknowledgements: This work was financially supported by the Slovenian Research Agency

(ARRS) under the bilateral project for scientific cooperation between Republic of Slovenia and Israel (NI-0002). Ms. T. Chouki acknowledges the scholarship provided by the Public Scholarship, Development, Disability and Maintenance Fund of the Republic of Slovenia (Ad futura program) for PhD studies at the University of Nova Gorica. Dr. B. Donkova is grateful to the EU Operational Programme “Science and Education for Smart Growth”, project BG05M2OP001-2.009-0028, for making possible to realize a visit for joint research at the University of Nova Gorica.

REFERENCES

1. H. Du, S. Gu, R. Liu, C. M. Li, *Int J Hydrogen Energy*, **40**, 14272 (2015).
2. X. Peng, A. M. Qasim, W. Jin, L. Wang, L. Hu, Y. Miao, W. Li, Y. Li, Z. Liu, K. Huo, K. Y. Wong, P. K. Chu, *Nano Energy*, **53**, 66 (2018).
3. E. J. Popczun, C. G. Read, C. W. Roske, N. S. Lewis, R. E. Schaak, *Angew. Chemie – Int. Edn.*, **53**, 5427 (2014).
4. Z. Zhou, L. Wei, Y. Wang, H. E. Karahan, Z. Chen, Y. Lei, X. Chen, S. Zhai, X. Liao, Y. Chen, *J. Mater. Chem. A*, **5**, 20390 (2017).
5. A. Adam, M. H. Suliman, H. Dafalla, A. R. Al-Arfaj, M. N. Siddiqui, M. Qamar, *ACS Sustain. Chem. Eng.*, **6**, 11414 (2018).
6. J. M. McEnaney, J. Chance Crompton, J. F. Callejas, E. J. Popczun, C. G. Read, N. S. Lewis, R. E. Schaak, *Chem. Commun.*, **50**, 11026 (2014).
7. Z. Gao, Q. Gao, Z. Liu, C. Zhang, X. Zhang, X. Liu, R. Wang, N. Li, *RSC Adv.*, **6**, 114430 (2016).
8. Q. Yang, R. Zhang, W. Wang, P. Zhou, L. Wang, T. Chen, H. Xu, L. Zheng, *Sustain. Energy Fuels*, **3**, 3078 (2019).
9. Y. Pei, Y. Cheng, J. Chen, W. Smith, P. Dong, P. M. Ajayan, M. Ye, J. Shen, *J. Mater. Chem. A*, **6**, 23220 (2018).
10. V. S. Milusheva, B. R. Tzaneva, M. C. Petrova, B. I. Stefanov, *Bulg. Chem. Commun.*, **5**, 15 (2020).
11. N. Coleman, M. D. Lovander, J. Leddy, E. G. Gillan, *Inorg. Chem.*, **58**, 5013 (2019).
12. Y. Park, H. Kang, Y. Hong, G. Cho, M. Choi, J. Cho, D. Ha, *Int. J. Hydrogen Energy*, (2020) doi.org/10.1016/j.ijhydene.2020.03.051.
13. S. Cao, Y. Chen, C. C. Hou, X. J. Lv, W. F. Fu, *J. Mater. Chem. A*, **3**, 6096 (2015).
14. G. Cho, H. Kim, Y. S. Park, Y. K. Hong, D. H. Ha, *Int. J. Hydrogen Energy*, **43**, 11326 (2018).
15. J. F. Callejas, J. M. McEnaney, C. G. Read, J. C. Crompton, A. J. Biacchi, E. J. Popczun, T. R. Gordon, N. S. Lewis, R. E. Schaak, *ACS Nano*, **8**, 11101 (2014).
16. Y. Shi, Y. Xu, S. Zhuo, J. Zhang, B. Zhang, *ACS Appl. Mater. Interfaces*, **7**, 2376 (2015).
17. J. M. McEnaney, J. C. Crompton, J. F. Callejas, E. J. Popczun, A. J. Biacchi, N. S. Lewis, R. E. Schaak, *Chem. Mater.*, **26**, 4826 (2014).

18. J. Liu, M. Meyns, T. Zhang, J. Arbiol, A. Cabot, A. Shavel, *Chem. Mater.*, **30**, 1799 (2018).
19. J. Wang, Q. Yang, Z. Zude, *J. Phys. Chem. Lett.*, **1**, 102 (2010).
20. G. Li, Q. Yang, J. Rao, C. Fu, S. Liou, G. Auffermann, Y. Sun, C. Felser, *Adv. Funct. Mater.*, **30**, 1907791 (2020).
21. Z. Huang, Z. Chen, Z. Chen, C. Lv, M. G. Humphrey, C. Zhang, *Nano Energy*, **9**, 373 (2014).
22. J. Wang, A. C. Johnston-Peck, J. B. Tracy, *Chem. Mater.*, **21**, 4462 (2009).
23. T. Chouki, M. Machreki, S. Emin, *Int. J. Hydrogen Energy*, **45**, 21473 (2020).
24. L. Lutterotti, *Nucl. Instrum. Methods Phys. Res., B*, **268**, 334 (2010).
25. P. Paunović, O. Popovski, G. Načevski, E. Lefterova, A. Grozdanov, A. T. Dimitrov, *Bulg. Chem. Commun*, **50**, 82 (2018).
26. Y. Liang, Q. Liu, A. M. Asiri, X. Sun, Y. Luo, *ACS Catal.*, **4**, 4065 (2014).
27. Y. Yao, N. Mahmood, L. Pan, G. Shen, R. Zhang, R. Gao, F. Aleem, X. Zhang, J. J. Zou, *Nanoscale*, **10**, 21327 (2018).
28. R. Liu, S. Gu, H. Du, C. M. Li, *J. Mater. Chem. A*, **2**, 17263 (2014).
29. C. Y. Son, I. H. Kwak, Y. R. Lim, J. Park, *Chem. Commun.*, **52**, 2819 (2016).
30. M. Wang, R. Zhao, X. Li, X. Zhao, L. Jiang, *ChemNanoMat*, **5**, 593 (2019).
31. C. Lin, Z. Gao, J. Yang, B. Liu, J. Jin, *J. Mater. Chem. A*, **6**, 6387 (2018).
32. X. Zhu, M. Liu, Y. Liu, R. Chen, Z. Nie, J. Li, S. Yao, *J. Mater. Chem. A*, **4**, 8974 (2016).
33. L. Tian, X. Yan, X. Chen, *ACS Catal.*, **6**, 5441 (2016).
34. Y. Xu, R. Wu, J. Zhang, Y. Shi, B. Zhang, *Chem. Commun.*, **49**, 6656 (2013).
35. S. Emin, C. Altinkaya, A. Semerci, H. Okuyucu, A. Yildiz, P. Stefanov, *Appl. Catal. B Environ.*, **236**, 147 (2018).
36. T. Shinagawa, A. T. Garcia-Esparza, K. Takanabe, *Sci. Rep.*, **5**, 13801 (2015).